SEM Evaluation of the Effects of Laser-Mediated Implant Surface Decontamination: An In Situ Human Pilot Study

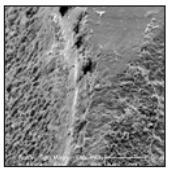

Eric Linden, DMD, MSD[1]
Charles M. Cobb, DDS, MS, PhD[2]
Paul Fletcher, DDS[3]
Donggao Zhao, PhD[4]

Successful treatment of peri-implantitis requires decontamination of implant surfaces exposed to biofilms and byproducts of tissue inflammation. In this regard, dental lasers may provide a clinical benefit. While the inherent characteristics of specific laser wavelengths may damage titanium implant surfaces, in vitro and animal studies have shown that damage to the target surface can be avoided with the selection of appropriate laser parameters. In this in situ human study, five hopeless implants were irradiated, each by one of the following lasers: Nd:YAG (1,064 nm), Er,Cr:YSGG (2,780 nm), Er:YAG (2,940 nm), CO_2 (9,300 nm), and CO_2 (10,600 nm) at their recommended settings. All implants were then removed and examined under scanning electron microscopy for the presence of residual bacteria and to assess the extent of damage to the implant surface. An additional implant (implant no. six) was irradiated and evaluated by the Limulus Amebocyte Lysate test for the presence of residual lipopolysaccharide endotoxin. The results showed that while there were localized areas of heat-related damage to an implant surface following laser irradiation, residual bacteria were rarely noted. Additionally, the Limulus Amebocyte Lysate test indicated a nearly complete removal of endotoxin. With the use of appropriate settings, all current dental lasers can be utilized for implant surface decontamination in a human.
Int J Periodontics Restorative Dent 2021;41:711–717. doi: 10.11607/prd.4911

[1]Columbia University College of Dental Medicine, New York, New York, USA.
[2]Professor Emeritus, Department of Periodontics, School of Dentistry, University of Missouri–Kansas City, Kansas City, Missouri, USA.
[3]Stony Brook University School of Dental Medicine, Stony Brook, New York, USA.
[4]Electron Microscope Laboratory, School of Dentistry, University of Missouri–Kansas City, Kansas City, Missouri, USA.

Correspondence to: Dr Eric Linden, 595 Chestnut Ridge Rd, Suite 7, Woodcliff Lake, NJ 07677-7667, USA. Fax: 201-307-0044. Email: drericlinden@drgums.com

Submitted March 2, 2020; accepted May 8, 2020.
©2021 by Quintessence Publishing Co Inc.

Peri-implantitis is characterized by bleeding on probing, purulence elicited by probing or gingival palpation, increased pocket probing depth beyond a baseline measurement, and radiographic evidence of continued bone loss after 1 year of functional loading.[1] If left untreated, this bone loss has been shown to increase exponentially, especially in patients with predisposing factors like a prior history of periodontal disease.[2–4]

Treatment consists of implant surface decontamination to eliminate the bacterial biofilm or reduce it to a subinflammatory concentration. Additionally, the implant surface oxide layer must be free of residual contaminants, such as lipopolysaccharide bacterial cell wall endotoxin.[5,6] This level of decontamination will optimize the potential for soft tissue re-adherence and a subsequent reduction in pocket probing depth and bleeding on probing. If the configuration of the bony defect permits, osseous regeneration, using an open flap technique, can also be performed concomitant with the surface-decontamination procedure. While there is no consensus on the ideal method for implant surface decontamination, an assortment of techniques have been used, including the use of dental lasers.[6–9]

Dental lasers have recently been suggested to offer clinical

© 2021 BY QUINTESSENCE PUBLISHING CO, INC. PRINTING OF THIS DOCUMENT IS RESTRICTED TO PERSONAL USE ONLY.
NO PART MAY BE REPRODUCED OR TRANSMITTED IN ANY FORM WITHOUT WRITTEN PERMISSION FROM THE PUBLISHER.

benefit for implant surface decontamination. Lasers with different wavelengths and having different clinical applications were introduced to dentistry over 50 years ago and have been used primarily for ablation and recontouring of oral soft tissue, hard tooth structure, and bone, and for achieving better control of bleeding, swelling, and discomfort levels than achieved when using a scalpel or dental drill.[10,11]

The lasers and wavelengths most commonly used in dentistry are diode laser (810 to 980 nm), Nd:YAG (1,064 nm), Er,Cr:YSGG (2,780 nm), Er:YAG (2,940 nm), CO_2 (9,300 nm), and CO_2 (10,600 nm). Depending on the wavelength and the target tissue or material, the laser energy beam may be reflected, transmitted, scattered, or absorbed. The target's absorption of laser energy, dependent on selected parameters, can produce desired effects such as hemostasis, thermal ablation or vaporization, and photoacoustic hard tissue destruction.[10]

The inherent characteristics of a specific laser wavelength have the potential to damage implant surfaces. Use of any laser, regardless of wavelength, with the improper choice of parameters can produce undesired sequelae (eg, excessive heat buildup that, in turn, leads to thermal damage, carbonization or charring of soft and/or hard tissue, and irreparable alterations of the implant surface).[10,11] However, in vitro and animal studies have shown that with the appropriate selection of laser parameters (ie, exposure time, use of continuous or intermittent delivery of the energy beam, delivery tip design and diameter, use of focused or defocused energy beam, and wattage or energy output of the laser),[10] adverse effects to target surfaces can be avoided during implant surface decontamination.

Several previous investigations[12–17] using a variety of methodologies have reported on the application of the Er:YAG, Er,Cr:YSGG, and 10,600-nm CO_2 lasers for in situ treatment of peri-implantitis. However, the results are equivocal or conflicted. Additionally, several recent systematic reviews[18–22] were consistent in concluding that the application of lasers in peri-implantitis treatment provides minimal clinical benefit.

The present study utilized five lasers: Nd:YAG (Nd; PerioLase MVP-7 laser, LAPIP Protocol, Millennium Dental Technologies); Er,Cr:YSGG (ECr; Waterlase iPlus, Biolase Repair Protocol, Biolase); Er,YAG (EYAG; AdvErl EVO, J. Morita); 9,300-nm CO_2 (C9.3; Solea 9.3-µm CO_2 laser, Convergent Dental); and 10,600-nm CO_2 (C10.6; LS-1005 CO_2 laser, LightScalpel) at prescribed settings to decontaminate six hopeless implants distributed among five patients. The implants were atraumatically removed, and five of the implants were examined by scanning electron microscopy (SEM) for the presence of residual bacteria and to assess the extent of damage, if any, to the implant surface. The sixth implant was evaluated by the Limulus Amebocyte Lysate test for the presence of residual lipopolysaccharide endotoxin.

Materials and Methods

Six failing implants, distributed among five patients, were treatment-planned for removal due to three or more of the following criteria: *(1)* bleeding on probing, *(2)* purulence elicited by probing or gingival palpation, *(3)* radiographic evidence of advanced, progressive bone loss, *(4)* mobility of the implant body, and/or *(5)* persistent infection and pain. Each patient consented to laser treatment of the failing implant prior to its atraumatic removal and were aware it may be used for publication purposes.

A total of five specimens were examined by SEM. Each implant was treated with a different laser wavelength using the following closed protocol and parameters:

Specimen 1: Nd (1,064 nm)

Step 1: Laser epithelial ablation (settings: 100 msec, 4 W, and 20 Hz for a total of 75 J). Step 2: Piezoscaler (Piezon 250, EMS) debridement (using the P tip) of the implant using a 50:50 mixture of chlorhexidine and sterile water until the operator felt the implant surface was adequately debrided. Step 3: Blunt dissection of the pocket tissue using the tip of the P tip until the attachment was dissected down to the osseous crest circumferentially (360 degrees around the entire implant). Step 4: Laser hemostasis (settings: 550 msec, 4 W, and 20 Hz for a total of 30 J).

© 2021 BY QUINTESSENCE PUBLISHING CO, INC. PRINTING OF THIS DOCUMENT IS RESTRICTED TO PERSONAL USE ONLY.
NO PART MAY BE REPRODUCED OR TRANSMITTED IN ANY FORM WITHOUT WRITTEN PERMISSION FROM THE PUBLISHER.

Specimen 2: ECr (2,780 nm)

Step 1: Deepithelialization of the outer pocket using the PFTP5 tip (1.5 W, air/water ratio of 40%/50%, pulse rate 30 Hz, H mode). Step 2: Sulcular debridement/degranulation using the RFTP5 tip (1.5 W, air/water ratio of 40%/50%, pulse rate 30 Hz, H mode). Step 3: Bone decortication using the MZ6 tip (2.5 W, air/water ratio of 40%/50%, 30 Hz, H mode). Step 4: Sulcular debridement using the RFTP5 tip (1.5 W, air/water ratio of 10%/10%, pulse rate 75 Hz).

Specimen 3: EYAG (2,940 nm)

Step 1: Degranulation/debridement using the PS600T tip (20 pps, 40 to 50 mJ, water/air ratio of 7/10). Step 2: Decontamination of implant surface using the R600T tip (20 pps, 40 to 50 mJ, water/air ratio of 7/10).

Specimen 4: C9.3 (9,300 nm)

Step 1: Modified fiberotomy using a small no. 7 elevator (unpublished data by E. Linden and R. Cantor). Step 2: Laser deepithelialization/decontamination using a 1.25 spot size (15/600 tip, 20% governor speed, 1% mist).

Specimen 5: C10.6 (10,600 nm)

Step 1: Modified fiberotomy using a small no. 7 elevator to open up the crest of tissue surrounding the implant.[12] Step 2: Laser sulcular debridement/deepithelialization with air purge on the high setting, using a 0.25-mm ceramic tip (super pulse mode, 2 W). Step 3: Piezo P tip to clean and remove contaminants on the implant surface. Step 4: Lasering with a 0.25-mm ceramic tip (super pulse mode, air purge on the high setting, 2 W).

Evaluation

Immediately after removal, each of the five specimens dedicated for SEM evaluation was immersed in 10% neutral buffered formalin and shipped to the University of Missouri–Kansas City, School of Dentistry, Electron Microscope laboratory. Upon arrival, specimens were immediately rinsed three times in 0.1-M cacodylate buffer (pH 7.4) for 5 minutes per rinse. Following the buffer rinse, specimens were dehydrated in a series of graded ethanol solutions (20% to 100%) at 5-minute intervals and then immersed in hexamethyldisilazane for 30 minutes. Each specimen was then affixed to an aluminum stub and stored in a desiccator overnight, followed by sputter coating with approximately 20 nm of gold palladium. Specimens were examined in a XL30 ESEM-FEG scanning electron microscope (FEI) at various magnifications ranging from ×26 to ×16,000. Low magnifications were utilized for orientation purposes, and higher magnifications were utilized for identification of residual microbes by morphotype (ie, coccus; short, medium, and long rods; and fusiform, spirochete-like, and curved rods).

The sixth failed implant was atraumatically removed, immediately irradiated with a C9.3 laser (using the same protocol as previously noted), and placed in an empty sterile vial. This vial was then submitted for Limulus Amebocyte Lysate test, an in vitro assay to detect and quantify lipopolysaccharide bacterial endotoxin, a component of gram-negative bacteria in the cell wall.

Results

All failed implants were laser-treated using a closed protocol (ie, lasers were inserted into the peri-implant pocket, and no surgical flaps were reflected). As a result of the closed protocol, it was not unexpected to find areas of the implant surfaces covered with adherent connective tissue, bone, and blood clots (Figs 1 and 2).

Mechanical instrumentation–induced surface damage (forceps) was apparent on two of the implants. Such damage involved the crest of threads and was the result of crushing and smearing the surface (Figs 3 and 4). Only one specimen exhibited heat-related surface damage resulting from laser irradiation.

The ECr-treated specimen showed complete decontamination of the implant surface when viewed at ×500 and ×1,000 magnifications, but showed relatively small areas of localized surface damage, and porous globules were visible, indicating melting and resolidification of bone hydroxyapatite mineral (Figs 5 and 6). The dimensions of such areas ranged from 100 to 300 μm^2. The implant surface immediately adjacent to the damaged bone also

© 2021 BY QUINTESSENCE PUBLISHING CO, INC. PRINTING OF THIS DOCUMENT IS RESTRICTED TO PERSONAL USE ONLY.
NO PART MAY BE REPRODUCED OR TRANSMITTED IN ANY FORM WITHOUT WRITTEN PERMISSION FROM THE PUBLISHER.

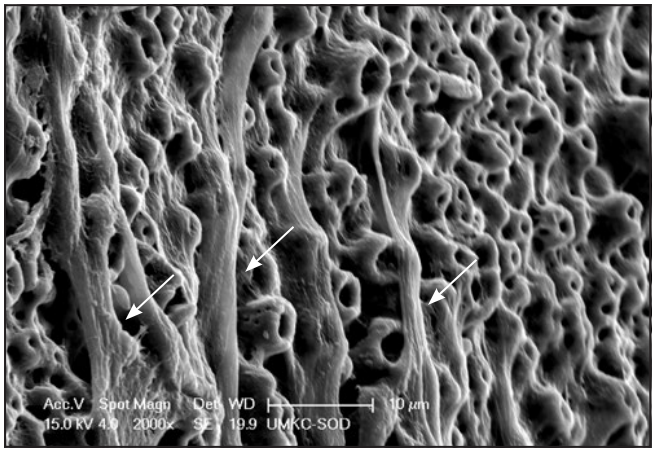

Fig 1 *SEM view of an implant surface treated with the EYAG laser. The specimen shows adherent parallel-running connective tissue fibers with a morphology characteristic of collagen* (arrows). *Original magnification ×2,000. Scale bar = 10 μm.*

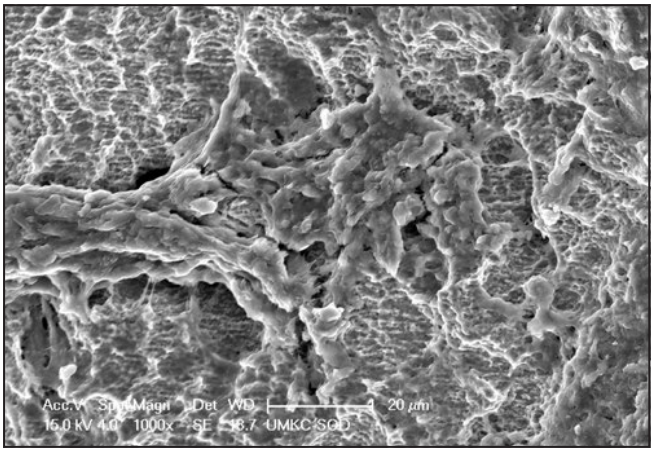

Fig 2 *SEM view of an implant surface treated with the C9.3 laser. The specimen shows adherent residual bone with a lobular morphology consistent with mineral deposition on a type I collagen matrix. Original magnification ×1,000. Scale bar = 20 μm.*

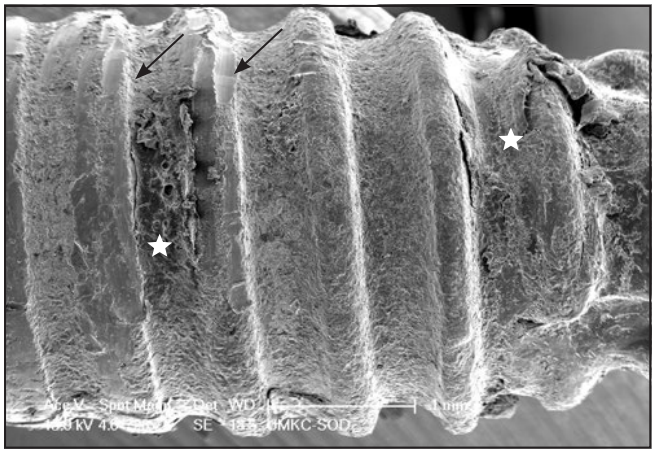

Fig 3 *SEM view of an implant surface treated with the C9.3 laser. The specimen shows surface damage from grasping the implant with forceps during removal* (arrows). *Residual bone in valleys between threads can also be seen* (stars). *Original magnification ×28. Scale bar = 1 mm.*

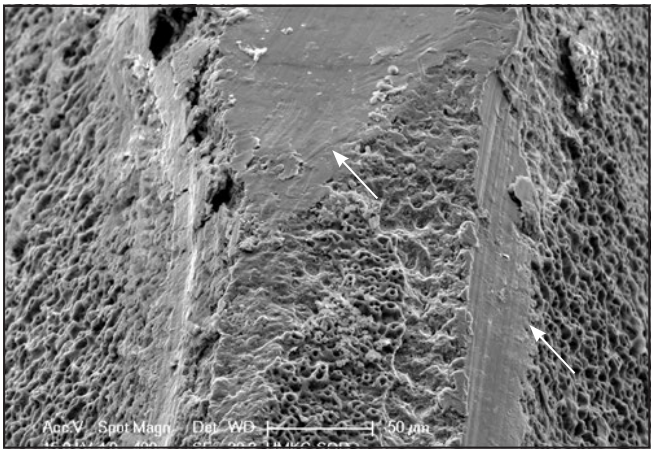

Fig 4 *SEM view of an implant surface treated with the C10.6 laser. The specimen shows crushed thread crests and smearing of titanium* (arrows) *resulting from grasping the implant with forceps during removal following treatment. Original magnification ×400. Scale bar = 50 μm.*

appeared to have been affected, featuring evidence of surface melting and extensive porosity (Fig 6).

The C9.3 SEM images showed complete bacterial decontamination with areas of adherent fibrous connective tissue. Residual bone exhibited a honeycomb-like appearance that was consistent in texture with an etching effect. The Nd images also show complete bacterial decontamination with no evidence of heat-induced surface damage. Interestingly, residual bone adhering to the implant surface that was exposed to Nd laser irradiation displayed a honeycomb-like etched surface, similar to the implant surface of the C9.3-treated implant (Fig 7).

Residual bacteria or intact biofilm was rarely noted during the SEM examination. Only one treated implant specimen, the C10.6 (Fig 8), exhibited randomly dispersed small aggregates of individual bacteria. While no bacteria were evident on the surface of the EYAG, clotted blood, fibrin, collagen fibers, and some areas of attachment were visible in the SEM images.

For finished medical devices, an endotoxin limit of no more than 20 EU/device is acceptable. The

© 2021 BY QUINTESSENCE PUBLISHING CO, INC. PRINTING OF THIS DOCUMENT IS RESTRICTED TO PERSONAL USE ONLY.
NO PART MAY BE REPRODUCED OR TRANSMITTED IN ANY FORM WITHOUT WRITTEN PERMISSION FROM THE PUBLISHER.

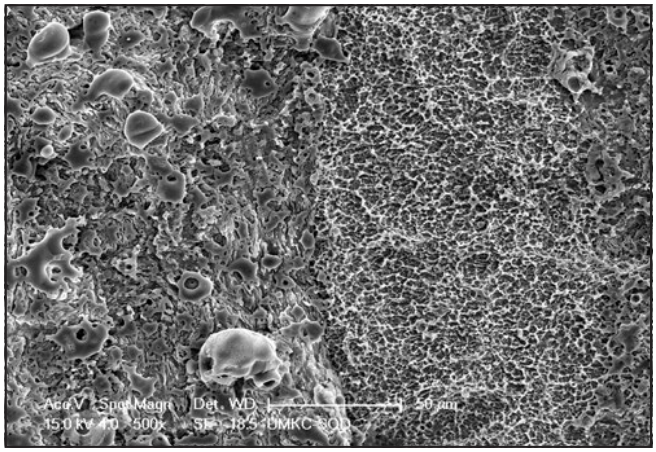

Fig 5 *SEM view of an implant surface exhibiting heat-induced damage to the bone and implant surface following treatment with the ECr laser. The left half of SEM image shows a porous globular morphology characteristic of melted and resolidified hydroxyapatite mineral. The upper right corner (magnified in Fig 6) is an area of melted titanium surface. Original magnification ×500. Scale bar = 50 µm.*

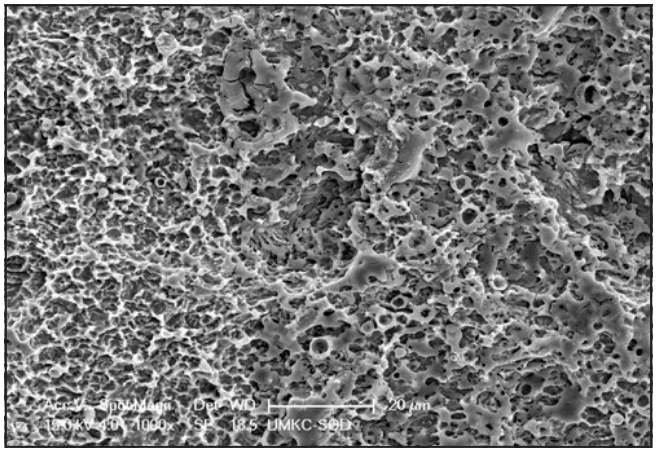

Fig 6 *A higher-magnification SEM view of the Fig 5 specimen shows heat-induced melting of the titanium surface following treatment with the ECr. Original magnification ×1,000. Scale bar = 20 µm.*

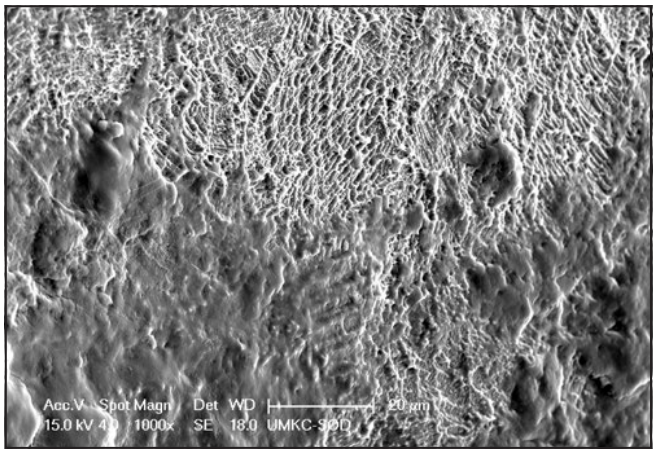

Fig 7 *SEM view of an implant surface with residual bone following treatment with the Nd laser. The specimen's undamaged bone (bottom half of photo) exhibits a relatively smooth surface. In contrast, the area of bone irradiated by the laser exhibits an etched honeycomb-like textured surface (top half of photo). Original magnification ×1,000. Scale bar = 20 µm.*

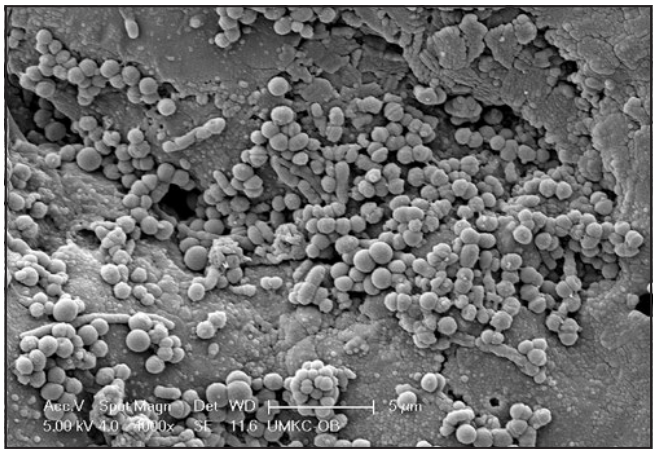

Fig 8 *SEM view of an implant surface treated with the C10.6 laser. The specimen shows an aggregate of residual coccoid and short rod bacterial morphotypes. Original magnification ×4,000. Scale bar = 5 µm.*

kinetic turbidimetric results of the Limulus Amebocyte Lysate test for the submitted implant (no. 6) was 0.382 EU/device. Assuming the presence of endotoxin on the implant surface prior to laser treatment, this result indicates nearly a compete removal of endotoxin.

Discussion

The present in situ implant decontamination study demonstrated that five different lasers used as a monotherapy or with the adjunctive addition of a piezoscaler were effective protocols for implant decontamination without causing significant surface damage. However, in light of the small sample size, it is important to emphasize caution in drawing definitive conclusions. The closed laser irradiation procedures performed on the hopeless implants followed established protocols provided by

© 2021 BY QUINTESSENCE PUBLISHING CO, INC. PRINTING OF THIS DOCUMENT IS RESTRICTED TO PERSONAL USE ONLY.
NO PART MAY BE REPRODUCED OR TRANSMITTED IN ANY FORM WITHOUT WRITTEN PERMISSION FROM THE PUBLISHER.

the manufacturer or were based on results from in vitro investigations conducted by the authors for the C10.6[12] and unpublished data for the C9.3.

This study required that two criteria be fulfilled to establish laser protocol efficacy: *(1)* no overheating of the implant, surrounding bone, or soft tissue, and *(2)* no detrimental damage to the implant surface. Prior to conducting this study, efficacy and safety testing were conducted on a porcine jaw immersed in a water bath and on bovine oral tissue with thermocouplers to monitor the heat generated from irradiation of the implant surface, the internal aspect of the implant body, and the surrounding bone. Additionally, stereoscopic microscopy was used to assess damage to the implant surface.

The human samples showed minor variations in the SEM images. In general, while all of the human samples appeared to have been effectively decontaminated (as judged by the lack of residual bacteria), relatively large surface areas of the implants were covered by blood clots, collagen, and adherent bone. As a result, the underlying implant structures covered with host tissues were not available for inspection to determine whether residual bacteria or biofilm were present.

Although the implant surface treated with the C10.6 laser was mostly free of bacteria, small aggregates of rods and cocci were visible, as were localized areas of manual instrument–induced damage. Thus, even with meticulous technique, adherent bacteria may remain on an implant surface. The clinical significance of this observation can only be answered with further study.

The C9.3 SEM images showed complete bacterial decontamination with areas of adherent fibrous connective tissue. The images suggest that the C9.3 laser is safe and effective in a closed environment.[23] All of the closed laser protocols in the present study utilized a hemostasis step with their respective wavelengths, and the results suggest that hemostasis began instantaneously. This biologic phenomenon seems to be the basis for potential regeneration around an implant, as the fibrin clot provides a scaffold for osteoblastic proliferation.

Whether melting of the implant surface is a significant deterrent for tissue regeneration requires further study. Both ECr and EYAG lasers have shallow-penetrating wavelengths. The ability to decontaminate an implant surface by superheating water and forcing a rapid phase transformation from liquid to gas results in micro-explosions, vaporizing the bacteria as the erbium wavelengths are absorbed. The ECr wavelength penetrates biologic target surfaces 3× deeper than the EYAG, which means it takes 3× longer to heat the target tissue or implant. This could explain the minimal amount of thermal damage that occurred with the EYAG laser compared to the ECr laser.[13]

Of all the lasers tested, the Nd had the deepest-penetrating wavelength.[10] It is clear from the present human study that if the practitioner follows a meticulous protocol and uses the Nd laser with the proper energy deposition (Joules), takes advantage of the Nd's favorable duty cycle, and utilizes proper cooling of the implant and surrounding tissues, this laser wavelength should not precipitate an adverse result despite the deeper penetrating qualities of the laser beam.

The result of the Limulus Amebocyte Lysate test indicated the absence of endotoxin from the surface of the test implant following irradiation with the C9.3 laser. While this is an important finding, the absence of an untreated control prohibits the conclusion of a definitive cause and effect relationship. Lipopolysaccharide endotoxin is heat-stable, and it has been known for some time that it is loosely adherent to root surfaces and is highly soluble in water.[24,25] Thus, the cooling mist of water that emanates from the handpiece during active use may, in fact, be responsible for removal of most of the endotoxin.

Conclusions

Results of this in situ human study constitute a proof-of-principle and demonstrate the potential use of each of the tested dental lasers in implant decontamination as part of a peri-implantitis treatment protocol. Further testing is indicated to confirm these results.

Acknowledgments

The authors declare no conflicts of interest.

© 2021 BY QUINTESSENCE PUBLISHING CO, INC. PRINTING OF THIS DOCUMENT IS RESTRICTED TO PERSONAL USE ONLY.
NO PART MAY BE REPRODUCED OR TRANSMITTED IN ANY FORM WITHOUT WRITTEN PERMISSION FROM THE PUBLISHER.

References

1. Renvert S, Persson GR, Pirih FQ, Camargo PM. Peri-implant health, peri-implant mucositis, and peri-implantitis: Case definitions and diagnostic considerations. J Periodontol 2018;89(suppl 1):s304–s312.
2. Berglundh T, Zitzmann NU, Donati M. Are peri-implantitis lesions different from periodontitis lesions? J Clin Periodontol 2011;38(suppl 11):188–202.
3. Roccuzzo M, De Angelis N, Bonino L, Aglietta M. Ten-year results of a three-arm prospective cohort study on implants in periodontally compromised patients. Part 1: Implant loss and radiographic bone loss. Clin Oral Implants Res 2010;21:490–496.
4. Roccuzzo M, Bonino F, Aglietta M, Dalmasso P. Ten-year results of a three arm prospective cohort study on implants in periodontally compromised patients. Part 2: Clinical results. Clin Oral Implants Res 2012;23:389–395.
5. Mombelli A. Microbiology and antimicrobial therapy of peri-implantitis. Periodontol 2000 2002;28:177–189.
6. Renvert S, Roos-Jansåker A, Claffey N. Non-surgical treatment of peri-implant mucositis and peri-implantitis: A literature review. J Clin Periodontol 2008;35(8 suppl):305–315.
7. Gosau M, Hahnel S, Schwarz F, Gerlach T, Reichert TE, Bürgers R. Effect of six different periimplantitis disinfection methods on in vivo human oral biofilm. Clin Oral Implants Res 2010;21:866–872.
8. Subramani K, Wismeijer D. Decontamination of titanium implant surface and re-osseointegration to treat peri-implantitis: A literature review. Int J Oral Maxillofac Implants 2012;27:1043–1054.
9. Ntrouka VI, Slot DE, Louropoulou A, Van der Weijden F. The effect of chemotherapeutic gents on contaminated titanium surfaces: A systematic review. Clin Oral Implants Res 2011;22:681–690.
10. Cobb CM. Lasers in periodontics: A review of the literature. J Periodontol 2006;77:545–564.
11. Cobb CM. Lasers and the treatment of periodontitis: The essence and the noise. Periodontol 2000 2017;75:205–295.
12. Linden E, Vitruk P. SuperPulse 10.6µm CO_2 laser–assisted, closed flap treatment of peri-implantitis. Implant Pract 2015;8:30–34.
13. Diaci J, Gaspirc B. Comparison of Er:YAG and Er,Cr:YSGG lasers used in dentistry. J Laser Health Acad 2012;12:1–13.
14. Schwarz F, Sculean A, Rothamel D, Schwenzer K, Georg T, Becker J. Clinical evaluation of an Er: YAG laser for non-surgical treatment of peri-implantitis: A pilot study. Clin Oral Implants Res 2005;16:44–52.
15. Renvert S, Lindahl C, Roos Jansåker AM, Persson GR. Treatment of peri-implantitis using an Er:YAG laser or an air-abrasive device: A randomized clinical trial. J Clin Periodontol 2011;38:65–73.
16. Persson GR, Roos-Jansåker A-M, Lindahl C, Renvert S. Microbiologic results after non-surgical erbium-doped:yttrium, aluminum, and garnet laser or air-abrasive treatment of peri-implantitis: A randomized clinical trial. J Periodontol 2011;82:1267–1278.
17. Schwarz F, Nuesry E, Bieling K, Herten M, Becker J. Influence of an erbium, chromium-doped yttrium, scandium, gallium, and garnet (Er,Cr:YSGG) laser on the reestablishment of the biocompatibility of contaminated titanium implant surfaces. J Periodontol 2006;77:1820–1827.
18. Romanos G, Ko HH, Froum S, Tarnow D. The use of CO(2) laser in the treatment of peri-implantitis. Photomed Laser Surg 2009;27:381–386.
19. Ashnagar S, Nowzari H, Nokhbatolfoghahaei H, Yaghoub Zadeh B, Chiniforush N, Choukhachi Zadeh N. Laser treatment of peri-implantitis: A literature review. J Lasers Med Sci 2014;5:153–162.
20. Hur Y, Ogata Y. Insufficient evidence to support the use of laser therapy for peri-implantitis. J Am Dent Assoc 2016;147:369–371.
21. Lin GH, Suárez López Del Amo F, Wang HL. Laser therapy for treatment of peri-implant mucositis and peri-implantitis: An American Academy of Periodontology best evidence review. J Periodontol 2018;89:766–782.
22. Natto ZS, Aladmawy M, Levi PA Jr, Wang HL. Comparison of the efficacy of different types of lasers for the treatment of peri-implantitis: A systemic review. Int J Oral Maxillofac Implants 2015;30:338–345.
23. Fletcher P, Linden E, Cobb C, Zhao D, Rubin J, Planzos P. Efficacy of removal of residual dental cement by laser, ultrasonic scalers, and titanium curette: An in vitro study. Compend Contin Educ Dent 2021;42:e5–e9.
24. Checchi L, Pelliccioni GA. Hand versus ultrasonic instrumentation in the removal of endotoxins from root surfaces in vitro. J Periodontol 1988;59:398–402.
25. Nakib NM, Bissada NF, Simmelink JW, Goldstine SN. Endotoxin penetration into root cementum of periodontally healthy and diseased human teeth. J Periodontol 1982;53:368–378.

© 2021 BY QUINTESSENCE PUBLISHING CO, INC. PRINTING OF THIS DOCUMENT IS RESTRICTED TO PERSONAL USE ONLY.
NO PART MAY BE REPRODUCED OR TRANSMITTED IN ANY FORM WITHOUT WRITTEN PERMISSION FROM THE PUBLISHER.